Geophysical Research Letters

RESEARCH LETTER
10.1029/2018GL077825

Key Points:
- A first detailed investigation of upper ocean response to strong atmospheric cold pool events associated with the MJO is presented
- A rapid cooling of SST is produced by the intensified salinity stratification generated by heavy rain and by the enhanced sensible heat flux due to cold rain temperature
- A subsequent gradual SST recovery (warming) occurs due to the mixing of warmer waters below the mixed layer produced by strong winds

Supporting Information:
- Supporting Information S1
- Figure S1
- Figure S2
- Figure S3
- Figure S4
- Figure S5

Correspondence to:
S. Pei,
suyang.pei@tamucc.edu

Citation:
Pei, S., Shinoda, T., Soloviev, A., & Lien, R.-C. (2018). Upper ocean response to the atmospheric cold pools associated with the Madden-Julian Oscillation. *Geophysical Research Letters*, *45*, 5020–5029. https://doi.org/10.1029/2018GL077825

Received 8 MAR 2018
Accepted 12 MAY 2018
Accepted article online 18 MAY 2018
Published online 31 MAY 2018

Upper Ocean Response to the Atmospheric Cold Pools Associated With the Madden-Julian Oscillation

Suyang Pei[1], Toshiaki Shinoda[1], Alexander Soloviev[2], and Ren-Chieh Lien[3]

[1]Department of Physical and Environmental Sciences, Texas A&M University-Corpus Christi, Corpus Christi, TX, USA, [2]Department of Marine and Environmental Sciences, Nova Southeastern University, Dania Beach, FL, USA, [3]Applied Physics Laboratory, University of Washington, Seattle, WA, USA

Abstract Atmospheric cold pools are frequently observed during the Madden-Julian Oscillation events and play an important role in the development and organization of large-scale convection. They are generally associated with heavy precipitation and strong winds, inducing large air-sea fluxes and significant sea surface temperature (SST) fluctuations. This study provides a first detailed investigation of the upper ocean response to the strong cold pools associated with the Madden-Julian Oscillation, based on the analysis of in situ data collected during the Dynamics of the Madden-Julian Oscillation (DYNAMO) field campaign and one-dimensional ocean model simulations validated by the data. During strong cold pools, SST drops rapidly due to the atmospheric cooling in a shoaled mixed layer caused by the enhanced near-surface salinity stratification generated by heavy precipitation. Significant contribution also comes from the component of surface heat flux produced by the cold rain temperature. After the period of heavy rain, while net surface cooling remains, SST gradually recovers due to the enhanced entrainment of warmer waters below the mixed layer.

Plain Language Summary The Madden-Julian Oscillation (MJO) is an eastward traveling intraseasonal (30–60 days) disturbance of clouds, rainfall, and winds in the tropical atmosphere, which has a strong impact on the tropical and extratropical climate. Atmospheric cold pools are pools of air cooled by rain evaporation, moving downward and spreading out as gust front upon reaching the surface. During MJO events, cold pools are often observed and accompanied with heavy rain and strong winds, changing sea surface temperature (SST) substantially. As such changes could have large impacts on air-sea interaction, understanding oceanic processes that influence SST may lead to improving MJO prediction. This study provides a first detailed investigation of upper ocean response to strong atmospheric cold pools associated with the MJO. The analysis of the data collected during the international field campaign indicates a rapid SST drop and subsequent gradual recovery (warming) associated with strong cold pool events. We demonstrated key oceanic processes controlling SST fluctuations observed during the field campaign based on a series of numerical ocean model simulations. The important oceanic processes include strong salinity stratification created by heavy rain, the mixing of near-surface seawater with colder rainwater, and the mixing of cold surface water with warmer waters below.

1. Introduction

Atmospheric cold pools are frequently observed over the open oceans. They form as convective downdrafts caused by evaporation of rainwater that originates from above the atmospheric boundary layer. As the cooled air moves downward to the surface, it spreads out horizontally to form a gust front where secondary convection could be further triggered. Small cold pools sometimes are combined to form mesoscale features and typically last less than one day and span 10–200 km in diameter (Barnes & Garstang, 1982; de Szoeke et al., 2017; Saxen & Rutledge, 1998; Young et al., 1995; Zipser, 1977; Zuidema et al., 2012, 2017). Recent observational and modeling studies (Chen et al., 2016; de Szoeke & Edson, 2017; Feng et al., 2014, 2015; Kilpatrick & Xie, 2015; Rowe & Houze, 2015; Schlemmer & Hohenegger, 2014; Skyllingstad & de Szoeke, 2015; Terai & Wood, 2013; Torri & Kuang, 2016) suggest that cold pools play an important role in organizing convection during the development of the Madden-Julian Oscillation (MJO; Madden & Julian, 1971, 1972; Zhang, 2005). Thus, the adequate representation of the multiscale interaction processes associated with cold pools in models may lead to the improvement of MJO prediction (de Szoeke et al., 2017; DeMott et al., 2015; Feng et al., 2015; Qian et al., 1998; Rowe & Houze, 2015; Schlemmer & Hohenegger, 2014; Seigel & van den Heever, 2011; Tompkins, 2001; Torri et al., 2015).

During the Dynamics of the Madden-Julian Oscillation (DYNAMO) field campaign (Yoneyama et al., 2013), strong cold pools were frequently observed especially during the convective active phase of the MJO (Chen et al., 2016; de Szoeke et al., 2017; de Szoeke & Edson, 2017; Feng et al., 2015; Yokoi et al., 2014). They largely increase surface fluxes by enhancing the wind speed and air-sea temperature difference. Observations from R/V *Revelle* (0°, 80°E) show that cold pools increase turbulent (sensible and latent) heat fluxes by 20 W/m^2 during the MJO active phase and 1.5 W/m^2 in the MJO suppressed phase (de Szoeke & Edson, 2017). The mean latent heat flux during the period of cold pools is about 140 W/m^2, compared to the mean latent heat flux of 110 W/m^2 for the entire period of the observations (de Szoeke et al., 2015; de Szoeke & Edson, 2017), and thus, cold pools can produce significant increase of the latent heat flux anomaly. Such an increase could be a large source of moisture anomaly for destabilizing the MJO convection based on the moist static energy budget analysis (de Szoeke et al., 2015; Riley Dellaripa & Maloney, 2015; Sobel et al., 2014). As cold pools are shown to strongly modulate sea surface temperature (SST) during the MJO events (de Szoeke & Edson, 2017; Moum et al., 2016) and the systematic error in SST could be one of the major causes of unsatisfactory MJO prediction (DeMott et al., 2015; Fu et al., 2018; Pujiana et al., 2018), a better understanding of processes controlling SST associated with cold pools could largely benefit MJO simulations and prediction.

While the importance of cold pools for surface heat fluxes is demonstrated in previous studies, upper ocean processes associated with cold pools, which are fundamental in determining the SST, have not been investigated. In this study, we present a first detailed investigation of upper ocean response to strong atmospheric cold pool events associated with the MJO. During these events, temperature inversion exists below the surface mixed layer. Analyses of the DYNAMO data and ocean model simulations reveal that surface fluxes and entrainment of warmer waters from below play an important role in modulating SST during its rapid cooling and subsequent recovery phase associated with cold pools. A particular emphasis of the analysis is given to the relative importance of the near-surface stable stratification produced by heavy rain and surface heat flux modified by the cold rain temperature for contributing to the rapid decrease of SST and the role of entrainment warming during the SST recovery phase.

2. Data and Model Simulations

2.1. Observation and Cold Pool Event

The data collected by the DYNAMO surface mooring located at 1°30′S, 78°45′E are used in this study. A detailed description of the data is found in Chi et al. (2014). A few strong cold pool events associated with intense precipitation and strong winds are selected for examining the upper ocean processes. One of such strong events occurred during 09:00 27 October 2011 to 09:00 28 October 2011 GMT (14:00 27 October 2011 to 14:00 28 October 2011 local standard time) within the active phase of the MJO event observed in late October (Chi et al., 2014). Similar cold pool events were also observed by R/V *Revelle* (de Szoeke et al., 2015), which is located at 0°, 80°E. They are possibly related to the large convective mesoscale systems during the active phase of the MJO. As shown in the following sections, the rapid cooling and slow recovery of surface air temperature measured by the surface mooring as well as the enhanced sensible and latent heat fluxes are all consistent with the observations at R/V *Revelle* (de Szoeke & Edson, 2017; Moum et al., 2014). Since this event includes a large SST drop associated with heavy precipitation and subsequent SST recovery, which are often found in other strong cold pool events, thorough analysis and a series of model simulations are conducted for the period of this event. Two other strong cold pool cases are shown in Figures S3 and S4, in which the same physical processes discussed in the following sections are identified.

2.2. Numerical Model Simulations

We use one-dimensional (1-D) high-resolution ocean models to examine the upper ocean processes associated with cold pools. Various mixing parameterizations based on different modeling philosophies are tested, including a bulk mixing model (Price et al., 1986; referred to as PWP model hereafter), K-profile parameterization (Large et al., 1994; referred to as KPP model hereafter), an empirical model based on gradient Richardson number (Soloviev et al., 2001; referred to as SLH model hereafter), and a second-order closure model with generalized length scale (Umlauf & Burchard, 2003; referred to as GL model hereafter). KPP model and GL model are tested using the General Ocean Turbulence Model (GOTM; Burchard et al., 1999; Umlauf et al., 2005).

The model depth is 100 m, with a vertical grid interval of 0.5 m. The period of the model simulations is 24 hr with a time step of 0.5 s. Models are forced by hourly surface fluxes calculated using meteorology measurements on the moorings (including measured downward shortwave radiation and adjusted downward longwave

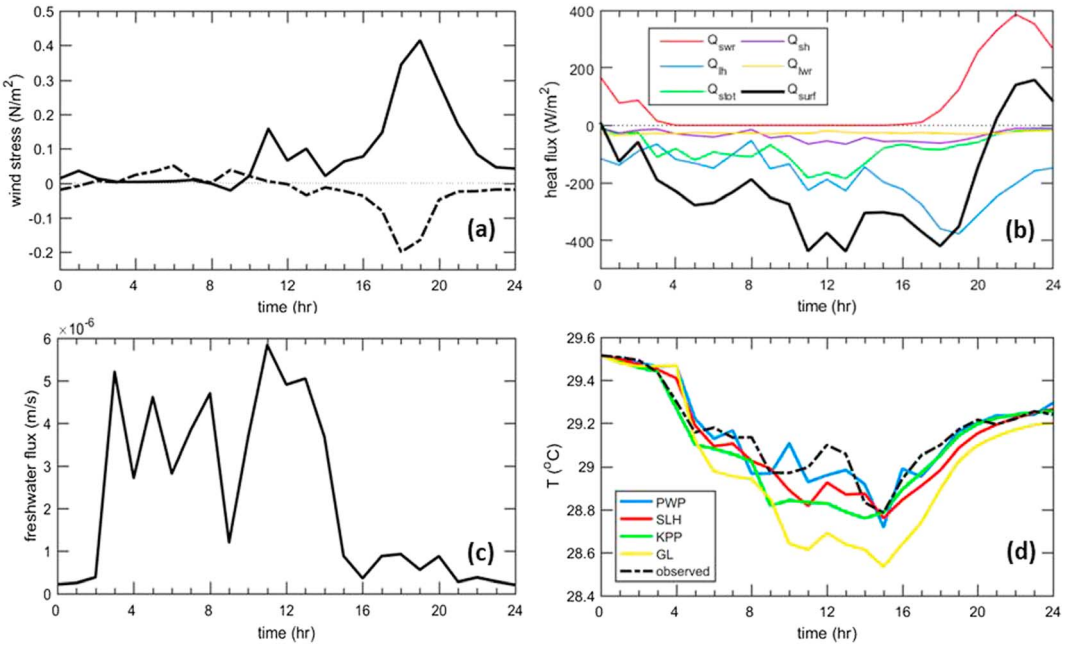

Figure 1. (a) Time series of surface freshwater flux (precipitation minus evaporation) in the cold pool event period from 09:00 27 October 2011 to 09:00 28 October 2011 GMT (14:00 27 October 2011 to 14:00 28 October 2011 local standard time). Positive values indicate precipitation exceeding evaporation. (b) Time series of zonal (solid line) and meridional (dashed line) wind stresses. (c) Time series of shortwave radiation Q_{swr} (red line), latent heat flux Q_{lh} (blue line), sensible heat flux Q_{stot} (green line), sensible heat flux without the cold rain effect Q_{sh} (purple line), longwave radiation Q_{lwr} (dark yellow line), and net surface heat flux Q_{surf} (black line). Positive values indicate heating the ocean. (d) Time series of SST from observation (black dash line), PWP model (blue line), SLH model (red line), KPP model (green line), and GL model (yellow line).

radiation; Chi et al., 2014) applying the Coupled Ocean-Atmosphere Response Experiment (COARE) version 3.5 bulk flux algorithm (Edson et al., 2013; Fairall et al., 1996, 2003). The initial condition of velocity, temperature, and salinity is obtained from mooring observations. The amount of shortwave radiation absorbed in the ocean is approximated with double exponential functions for Jerlov water type IA (Paulson & Simpson, 1977). The *e*-folding length scale is 20 m, and 62% of the shortwave radiation is absorbed at the surface. We also use in situ optical profiles obtained from R/V *Revelle* (Moum et al., 2014) to compute the penetrative solar radiation. No significant difference is found between these two methods.

3. Results

Cold pools are generally associated with heavy rain and strong winds. Figures 1a and 1b show freshwater flux and wind stresses observed during the cold pool event on 27 October. Heavy precipitation is found during hours 3–14 with an average rain rate of 14.7 mm/hr, producing a strong freshwater flux of 4.0×10^{-6} m/s (Figure 1a). This heavy rain period is followed by a strong westerly wind burst occurred at hour 16, lasting about 6 hr. Zonal wind stress reaches its maximum 0.4 N/m^2 at hour 19 (Figure 1b).

Heavy rain and strong winds also modulate surface heat fluxes. The net surface heat flux Q_{surf} is negative (cooling the ocean) from hours 1 to 20 primarily due to enhanced latent heat flux Q_{lh}, and sensible heat flux Q_{stot} (Figure 1c). In addition to surface winds and the air-sea temperature difference at the surface, the negative sensible heat flux Q_{stot} (green line) is enhanced by bringing cold rainwater to the ocean. While this effect is negligible in most cases on a longer time scale, the extremely heavy rain associated with cold pools could significantly influence the net sensible heat flux. To quantify the impact of rain temperature on Q_{stot}, the sensible heat flux is calculated without including the effect of cold rain temperature using the COARE 3.5 bulk flux algorithm. Here the sensible heat flux without the effect of cold rain temperature is defined as Q_{sh}, and the portion of the sensible heat flux due to the cold rain temperature is defined as $Q_{rain} = Q_{stot} - Q_{sh}$, which is computed assuming that the temperature of raingrops is the wet bulb temperature (Gosnell et al.,

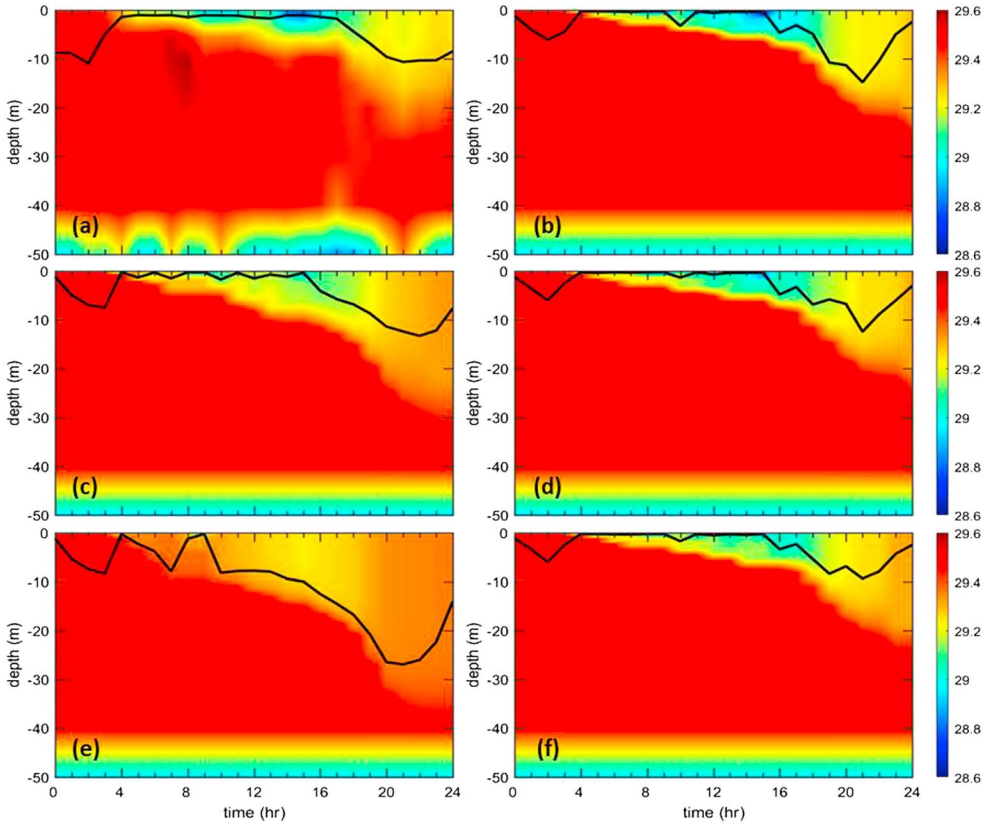

Figure 2. Temperature and the mixed layer depth (solid line) from (a) observation, (b) control simulation, (c) P1 simulation (50% precipitation of control simulation), (d) Q1 simulation (50% sensible heat flux due to cold rain temperature of control simulation), (e) P2 simulation (25% precipitation of control simulation), and (f) Q2 simulation (25% sensible heat flux due to cold rain temperature of control simulation). The mixed layer depth in observations is computed based on the density change of 3×10^{-2} kg/m^3 from the surface value. Simulations are conducted with PWP model.

1995). During the heavy rain period, Q_{rain} has an average value of −83 W/m^2, approximately twice of Q_{sh}, except at hour 9 when it becomes smaller than Q_{sh} because of a sudden decrease of precipitation (Figure S1a). During hours 10–14, Q_{stot} is nearly twice as that of hour 3–8 due to the increase of both Q_{rain} and Q_{sh}. The increase of Q_{rain} is a result of stronger precipitation, while the increase in Q_{sh} is due to the increase of wind speed and air-sea temperature difference during this period.

Strong winds accompanying the cold pools can significantly increase the latent heat flux (de Szoeke & Edson, 2017). The latent heat flux Q_{lh} (blue line in Figure 1c) is well correlated with the surface wind stress (Figure 1b). It increases from about 120 to 200 W/m^2 as a result of strong zonal wind during hours 10–14. It further increases by the following stronger winds, reaching its maximum of 377 W/m^2 at hour 19 when the wind speed is at its maximum. As a result of increasing latent heat flux, the net surface heat flux Q_{surf} is negative (cooling) until hour 21 when shortwave radiation exceeds the surface cooling (Figure 1c). The longwave radiation Q_{lwr} has an average value of 27 W/m^2 and is nearly constant in the entire period.

In summary, the net surface heat flux cools the ocean intensively due to the effect of heavy rain and strong wind bursts associated with the cold pool event. The sensible heat flux is comparable to the latent heat flux largely due to the cold rain temperature during the period of heavy precipitation. Once rain weakens, the sensible heat flux decreases, and strong winds significantly increase the latent heat flux, which dominates the surface cooling until shortwave radiation becomes significant.

During the period of heavy precipitation, the observed SST decreases rapidly by 0.73 °C in 15 hr, reaching its minimum 28.79 °C (Figure 1d). It then recovers gradually and continues to increase during the period of strong winds, returning to 29.24 °C at the end of the event. Along with the rapid SST decrease (0.73 °C) in this period, the surface air temperature drops by 4.8 °C (not shown), increasing air-sea temperature difference by nearly 4 times. Observed

Table 1
Summary of Sensitivity Simulations With Varying Precipitation P (P-Group) and Sensible Heat Flux Modified by Cold Rain Temperature Q_{rain} (Q-Group)

Sensitivity simulations	P/P^{ctr}	Q_{rain}/Q_{rain}^{ctr}
P1	0.5	1
P2	0.25	1
Q1	1	0.5
Q2	1	0.25

Note. The label "ctr" indicates the control simulation. Other surface forcing and parameters are kept the same as the control simulation.

SST variations are simulated reasonably well by the 1-D model with different turbulence parameterization schemes (Figure 1d). In particular, model results using PWP, SLH, and KPP parameterizations realistically capture the magnitude of the rapid SST cooling and subsequent warming. In this particular case, the model with GL parameterization overestimates the SST cooling because of insufficient turbulence entrainment mixing of warmer waters from below.

Time series of mooring observations of vertical temperature profile in the upper 50 m with the mixed layer depth (MLD) are shown in Figure 2a. During the heavy rain period, cooling occurs within a very shallow layer near the surface because of the strong salinity stratification produced by the large surface freshwater flux. This produced an extremely shallow surface mixed layer of about 1 m. Sea surface salinity decreases by about 1.1 practical salinity unit within this period due to the heavy precipitation (Figure S1b). The shallow cold layer then deepens sharply after the heavy rain period, and the SST gradually increases. In this phase, the SST warming is caused by the entrainment of warmer waters below the surface mixed layer exceeding the negative net surface heat flux (cooling the ocean). The maximum MLD is about 11 m at hour 21 when winds start weakening. The mixed layer then becomes shallower as the net surface heat flux changes to positive. The overall response of ocean to this strong cold pool event occurs within the upper 30 m, not reaching the thermocline at about 45 m.

Besides capturing SST variation well, PWP model also has reasonable agreement with the observations in simulating the time evolution of vertical temperature profile and MLD (Figure 2b). Because of its simplicity and good performance in this case, it is used for further sensitivity simulations to quantify the relative importance of physical processes modulating SST variations.

4. Sensitivity Simulations

The rapid cooling of SST discussed in the previous section can be enhanced by heavy rain due to two major effects (e.g., Anderson et al., 1998; Gosnell et al., 1995). The first effect is that heavy precipitation creates strong salinity stratification of the upper layer, making it more stably stratified despite the existing temperature inversion, and thus maintains a shallow mixed layer. During this period, the density stratification is mostly determined by salinity, which is shown in Figure S2 that describes the buoyancy frequency (N^2) calculated from density change due to salinity and temperature, respectively. The mixed layer cooling is enhanced by distributing surface heat flux (cooling) within a thin layer and by suppressing the entrainment of warmer waters below. The second effect is to increase the sensible heat flux due to cold rain temperature Q_{rain} as demonstrated in Figures 1c and S1a. Here the first effect is termed as salinity stratification effect and the second effect is termed as the cold rain temperature effect. To determine the relative importance of the two effects for the SST cooling, we carried out sensitivity simulations, investigating these effects separately.

A series of model simulations are conducted by changing the precipitation P, while the sensible heat flux is kept the same (referred to as P-group simulations hereafter). This quantifies the salinity stratification effect. Also, a suite of experiments with a different amount of rain temperature effect on the sensible heat flux Q_{rain} is performed (referred to as Q-group simulations hereafter). This evaluates the cold rain temperature effect. The PWP simulation with hourly fluxes computed from the observational data is referred to as the "control simulation." Table 1 lists precipitation and sensible heat flux produced by cold rain temperature used in P-group and Q-group simulations, which will be described in further details in the following sections. Sensitivity simulations are also conducted for other two strong cold pool cases using KPP and SLH models. Similar physical processes discussed in the following sections are identified, and they are not model dependent.

4.1. P-Group Simulations

In P-group simulations, only precipitation P is different in each experiment and all the other forcing and parameters remain the same as in the control simulation. In P1 and P2 simulations, 50% and 25% of precipitation from the control simulation for each time step is used to force the model respectively. Note that the sensible heat flux in P1 and P2 simulations are the same as the control simulation even though precipitation is different. As a result of the reduction of precipitation, the average freshwater flux is reduced to 1.97×10^{-6} m/s for

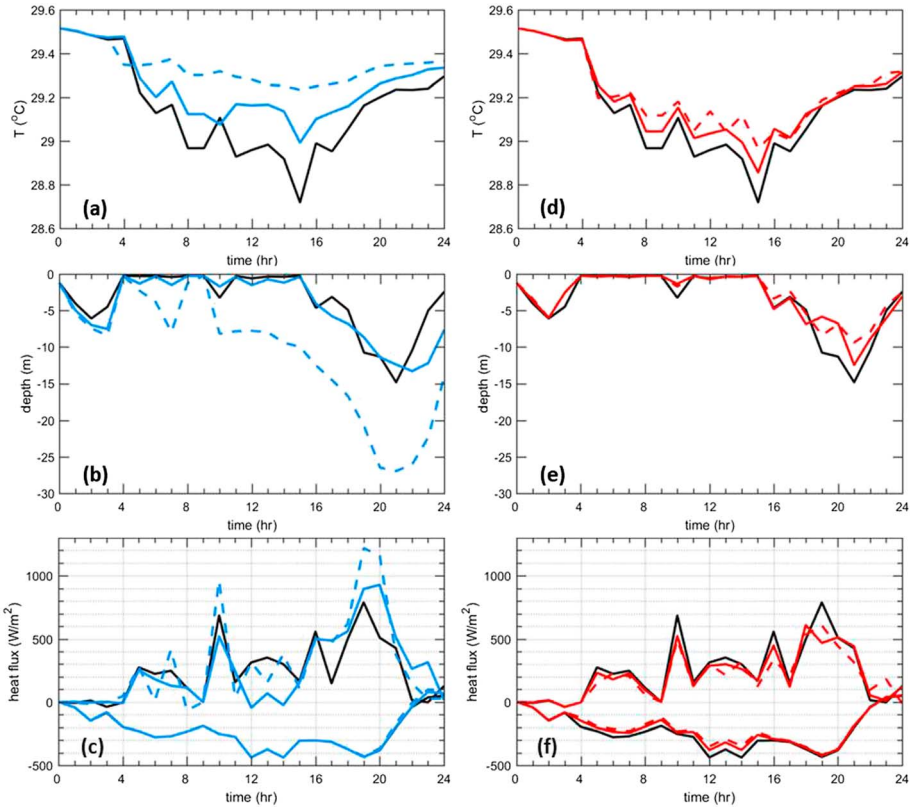

Figure 3. (a and d) Time series of SST, (b and e) mixed layer depth, and (c and f) hourly averaged surface and entrainment heat flux of sensitivity simulations. The results of varying precipitation (Figures 3a–3c). The blue solid lines indicate P1 simulation. The blue dashed lines indicate P2 simulation. The black lines indicate the control simulation. The results of varying sensible heat flux due to the rain temperature (Figures 3d–3f). The red solid lines indicate Q1 simulation. The red dashed lines indicate Q2 simulation. In (c) and (f), the top three lines represent the entrainment heat flux and the bottom three lines represent the net surface heat flux plus the penetrative component of shortwave radiation absorbed within the mixed layer. The bottom three lines in (c) are nearly identical. See text for the detail of the simulations.

P1 and 0.96×10^{-6} m/s for P2. Figures 2c and 2e show the time series of temperature profile with MLD from P1 and P2 simulations. Substantial differences in near-surface temperature and MLD between the control, P1, and P2 simulations are evident. During hours 4–15, the temperature is significantly higher and mixed layer is deeper in P1 and P2 than those in the control simulation, and the difference is much larger in P2. The impact of the precipitation is clearly evident in SST variation (Figure 3a). Compared to the control simulation, SST is higher in P1 by 0.27 °C and in P2 by 0.51 °C at hour 15.

One of the major reasons that produce the warmer SST in P1 and P2 simulations is the deeper mixed layer. In the control simulation, the cooling is concentrated in the extremely shallow mixed layer, while it is distributed to deeper layers in P1 and P2 simulations. A detailed MLD comparison of the P-group simulations is shown in Figure 3b. The shallowest MLD of about 0.3 m is found in the control simulation, whereas the shallowest MLD in P1 and P2 simulations is about 1 and 8 m, respectively.

The weaker salinity stratification also introduces a warming by the turbulent entrainment heat flux from below. Since the PWP model assumes bulk mixed layer (a constant temperature within the mixed layer), the entrainment heat flux can be accurately computed for each time step (e.g., Shinoda, 2005; Shinoda & Hendon, 1998). Following Shinoda (2005), the entrainment heat flux Q_{ent} is computed at each time step by integrating the heat equation:

$$Q_{ent} = \rho_0 c_p \int_0^h \frac{\partial T}{\partial t} dz - Q_0 \quad (1)$$

In which T is the mixed layer temperature, c_p is the specific heat of seawater, h is the MLD, and Q_0 is the net surface heat flux plus the penetrative component of shortwave radiation absorbed within the mixed layer.

Figure 3c shows the time series of Q_{ent} (top line) and Q_0 (bottom line). In P1 and P2 simulations, the entrainment warming is enhanced when significant change of MLD occurs during the period of heavy rain. For instance, at hour 10, the entrainment warming sharply increases as a result of the decrease of freshwater flux around hour 9 (Figure 1a) and the subsequent weakening of the stratification. It should be noted that Q_{ent} is not exactly zero when MLD does not change as shown in the control simulation around hours 4–8. This is because a gradient Richardson number adjustment is applied in each time step after the bulk Richardson number adjustment in PWP model to smooth out the temperature jump at the base of the mixed layer (Price et al., 1986). Therefore, even though the hourly averaged MLD stays the same, it produces a nonzero Q_{ent}.

In summary, P-group simulations demonstrate a substantial impact of heavy precipitation on the rapid SST cooling through strengthening of near-surface salinity stratification. As indicated by P2 and P1, intensified stable stratification produces a shallower mixed layer, enhancing the surface cooling by distributing it within the shallower mixed layer and suppressing the entrainment of warmer waters below the mixed layer.

4.2. Q-Group Simulations

In Q-group simulations, only the sensible heat flux modified by the cold rain temperature Q_{rain} varies in each simulation. Q1 and Q2 are forced with 50% and 25% Q_{rain} of the control simulation, respectively. The time series of temperature profile and MLD of Q1 and Q2 are shown in Figures 2d and 2f. The mixed layers remain very shallow in these two simulations, and the vertical structure of temperature is similar to the control simulation because of the large amount of freshwater flux (Figure 3e). However, SSTs of Q1 and Q2 are still significantly higher than the control simulation, as shown in Figure 3d. As discussed in P-group simulations, the very shallow mixed layer is a result of enhanced stable stratification due to heavy precipitation. Under such a stably stratified condition, the entrainment warming is suppressed (Figure 3f). The decrease of Q_{rain} is the only mechanism that drives the higher SST in S-group simulations. As demonstrated in Figure 1c, the cold rain temperature significantly influences the sensible heat flux during the cold pool event. For instance, Q1 simulation has average of about 41.5 W/m^2 increase of surface heat flux during hours 3–14. The resulting SST at hour 15 is 0.14 °C higher than the control simulation. In Q2 simulation, SST at hour 15 is higher than the control simulation by 0.25 °C. Therefore, the SST change due to the cold rain temperature effect is still significant, although the effect is less than that of the enhanced salinity stratification.

A possible influence of cold rain temperature on SST through the change of sensible heat flux has been suggested in few previous studies (e.g., Anderson et al., 1998). In this study, the DYNAMO in situ data and Q-group simulations quantify the effect of rain temperature and clearly demonstrate the significant contribution of the effect on SST variation during the cold pool events. While the sensible heat flux change caused by the cold rain temperature effect is generally a very small portion of the total sensible heat flux and thus its impact on SST is almost negligible, the results in this study indicate that the effect could be quite large during the heavy rain period of cold pool events. Q-group simulations demonstrate that the magnitude of SST cooling is reduced by about 30% by excluding the rain temperature effect (Figure 3d), suggesting that the cold rain temperature provides significant contribution to the SST change produced by strong cold pools.

4.3. Mixing Enhanced by Strong Wind Bursts

After the end of the heavy rain period, the SST starts to recover (warming) gradually (Figure 1d). However, the net surface heat flux is still negative (cooling), with a large value -400 W/m^2 due to the increase of latent heat flux caused by strong winds (Figure 1c). The SST warming during this period in the control simulation is primarily caused by substantial entrainment heat flux in hours 15–21 (Figure 3c). The mixed layer continues to deepen and reaches a maximum depth of 15 m at hour 21 (Figure 3b), generating a large amount of entrainment heat flux. The surface heat flux continues to be negative (cooling) even when insolation starts increasing at hour 16. It becomes positive near the end of the event at hour 21 when shortwave radiation exceeds the sum of other components of surface heat fluxes.

The results suggest that wind-induced mixing is the primary cause of the SST recovery (warming) during the cold pool event. The rapid deepening of the mixed layer from hours 15 to 18 is caused by a combination of the decrease of precipitation (Figure 1a) and strong winds (Figure 1b), generating a large entrainment heat flux (warming) (Figure 3c). From hours 19 to 21, mixed layer continues to deepen to its maximum depth while the entrainment heat flux decreases. Then the cooling of surface heat flux weakens remarkably due to the

increase of insolation and the decrease of latent heat flux. As a result, the SST continues to increase until the end of the event.

5. Conclusions and Discussion

Recent studies suggest that atmospheric cold pools play an important role in organizing convection during the MJO development (e.g., Chen et al., 2016; de Szoeke et al., 2015, 2017; de Szoeke & Edson, 2017; Feng et al., 2015; Rowe & Houze, 2015; Schlemmer & Hohenegger, 2014; Skyllingstad & de Szoeke, 2015). Atmospheric cold pools observed during the DYNAMO field campaign generated a substantial SST change through altering air-sea fluxes. Although the source of anomalous moisture during the MJO and thus the detailed mechanism how cold pools could impact the MJO is still uncertain (Riley Dellaripa et al., 2018; Zuidema et al., 2017), large changes in SST due to cold pools, such as those observed during DYNAMO, could have a large impact on the air-sea interactions. Thus, a better understanding of air-sea coupled processes associated with cold pools may lead to improving MJO simulations and prediction. However, previous studies mostly focus on atmospheric processes and air-sea fluxes. The associated ocean variability and oceanic processes, which could largely influence SST, have not been reported so far.

We present a first detailed study on the upper ocean response to cold pools through the analysis of in situ data collected during DYNAMO and a suite of 1-D ocean model simulations validated by DYNAMO observations. Primary ocean variability associated with strong cold pool event is characterized by a rapid and substantial decrease of SST followed by gradual recovery (warming). Such strong cold pool events are selected during DYNAMO observations to examine physical processes in the upper ocean. Surface fluxes estimated from DYNAMO observations reveal that heavy precipitation associated with cold pools provides a large amount of surface freshwater flux as well as significantly enhances the sensible heat flux due to the effect of cold rain temperature. The subsequent strong wind bursts after the period of heavy rain increase the latent heat flux, which continues to provide surface cooling until solar radiation exceeds the cooling.

Several 1-D ocean models are integrated with atmospheric forcing fields derived from DYNAMO observations described above. All models are able to simulate the observed rapid SST drop and gradual recovery reasonably well. Two groups of sensitivity simulations are performed using the PWP model to further distinguish the impact of heavy rain on the SST variation. One group quantifies the effect of near-surface salinity stratification by varying the amount of precipitation. The other group examines the effect of sensible heat flux modified by the cold rain temperature. These numerical experiments demonstrated that the rapid cooling of SST is enhanced primarily due to the intensified near-surface salinity stratification caused by the increased freshwater flux. It largely enhanced the cooling of SST through maintaining a very shallow mixed layer as well as the suppression of the entrainment of warmer waters below the mixed layer. The enhanced sensible heat flux produced by the colder rain temperature also significantly contributes to the rapid SST cooling.

During the subsequent wind bursts after the period of heavy rain, the warming (recovery) of the SST occurs primarily due to the enhanced mixing of warmer waters below the mixed layer produced by strong winds, although the surface heat flux continues to be negative (cooling) due to the increase of latent heat flux.

It is worth mentioning that the enhancement of SST cooling due to heavy precipitation has also been studied for tropical cyclones (e.g., Jacob & Koblinsky, 2013; Jourdain et al., 2013). While the strong salinity stratification impacts the SST cooling, the effect of cold rain temperature appears to have little influence on the cooling in the cold wake region. In contrast, this study suggests that the effect of rain temperature needs to be included for the accurate SST simulation probably due to the difference of surface MLDs in two cases. Unlike the tropical cyclone case, the very shallow mixed layer is maintained during the entire period of SST cooling for the cold pool case.

Finally, while this study demonstrates key oceanic processes controlling prominent SST changes associated with strong cold pools, the dominant processes may vary from event to event. Further studies that examine many other cold pool events, including weaker events, are necessary to better understand the overall impacts of cold pools on the air-sea interaction processes.

Acknowledgments
This research is supported by NOAA grant NA15OAR431074. T. Shinoda is also supported by NOAA grant NA17OAR4310256, NSF grants OCE-1658218 and AGS-1347132, and NASA grant NNX17AH25G. We would like to thank Carter Ohlmann for providing the in situ optical profile data obtained from R/V *Revelle*. The DYNAMO mooring measurements used in this paper can be found at https://www.eol.ucar.edu/field_projects/dynamo. Computing resources were provided partly by the HPC systems at the Texas A&M University (College Station and Corpus Christi). We thank the two anonymous reviewers for their insightful comments.

References

Anderson, S. P., Hinton, A., & Weller, R. A. (1998). Moored observations of precipitation temperature. *Journal of Atmospheric and Oceanic Technology*, *15*(4), 979–986. https://doi.org/10.1175/1520-0426(1998)015%3C0979:MOOPT%3E2.0.CO;2

Barnes, G. M., & Garstang, M. (1982). Subcloud layer energetics of precipitating convection. *Monthly Weather Review*, *110*(2), 102–117. https://doi.org/10.1175/1520-0493(1982)110%3C0102:SLEOPC%3E2.0.CO;2

Burchard, H., Bolding, K., & Villarreal, M. R. (1999). GOTM, a General Ocean Turbulence Model. Theory, implementation and test cases (Tech. Rep. EUR 18745 EN). Ispra, Italy: European Commission.

Chen, S. S., Kerns, B. W., Guy, N., Jorgensen, D. P., Delanoë, J., Viltard, N., et al. (2016). Aircraft observations of dry air, the ITCZ, convective cloud systems, and cold pools in MJO during DYNAMO. *Bulletin of the American Meteorological Society*, *97*(3), 405–423. https://doi.org/10.1175/BAMS-D-13-00196.1

Chi, N.-H., Lien, R.-C., D'Asaro, E. A., & Ma, B. B. (2014). The surface mixed layer heat budget from mooring observations in the central Indian Ocean during Madden-Julian Oscillation events. *Journal of Geophysical Research: Ocean*, *119*, 4638–4652. https://doi.org/10.1002/2014JC010192

de Szoeke, S. P., & Edson, J. B. (2017). Intraseasonal air-sea interaction and convection observed in DYNAMO/CINDY/AMIE and TOGA COARE. In *The Global Monsoon System: Research and Forecast* (pp. 349–364). Singapore: World Scientific.

de Szoeke, S. P., Edson, J. B., Marion, J. R., Fairall, C. W., & Bariteau, L. (2015). The MJO and air–sea interaction in TOGA COARE and DYNAMO. *Jounal of Climate*, *28*(2), 597–622. https://doi.org/10.1175/JCLI-D-14-00477.1

de Szoeke, S. P., Skyllingstad, E. D., Zuidema, P., & Chandra, A. S. (2017). Cold pools and their influence on the tropical marine boundary layer. *Journal of the Atmospheric Sciences*, *74*(4), 1149–1168. https://doi.org/10.1175/JAS-D-16-0264.1

DeMott, C. A., Klingaman, N. P., & Woolnough, S. J. (2015). Atmosphere-ocean coupled processes in the Madden-Julian oscillation. *Reviews of Geophysics*, *53*, 1099–1154. https://doi.org/10.1002/2014RG000478

Edson, J. B., Jampana, V., Weller, R. A., Bigorre, S. P., Plueddemann, A. J., Fairall, C. W., et al. (2013). On the exchange of momentum over the Open Ocean. *Journal of Physical Oceanography*, *43*(8), 1589–1610. https://doi.org/10.1175/JPO-D-12-0173.1

Fairall, C. W., Bradley, E. F., Godfrey, J. S., Wick, G. A., Edson, J. B., & Young, G. S. (1996). Cool-skin and warm-layer effects on sea surface temperature. *Journal of Geophysical Research*, *101*(C1), 1295–1308. https://doi.org/10.1029/95JC03190

Fairall, C. W., Bradley, E. F., Hare, J. E., Grachev, A. A., & Edson, J. B. (2003). Bulk parameterization of air–sea fluxes: Updates and verification for the COARE algorithm. *Journal of Climate*, *16*(4), 571–591. https://doi.org/10.1175/1520-0442(2003)016%3C0571:BPOASF%3E2.0.CO;2

Feng, Z., Hagos, S., Rowe, A. K., Burleyson, C. D., Martini, M. N., & de Szoeke, S. P. (2015). Mechanisms of convective cloud organization by cold pools over tropical warm ocean during the AMIE/DYNAMO field campaign. *Journal of Advances in Modeling Earth Systems*, *7*(2), 357–381. https://doi.org/10.1002/2014MS000384

Feng, Z., McFarlane, S. A., Schumacher, C., Ellis, S., Comstock, J., & Bharadwaj, N. (2014). Constructing a merged cloud-precipitation radar dataset for tropical convective clouds during the DYNAMO/AMIE experiment at Addu Atoll. *Journal of Atmospheric and Oceanic Technology*, *31*(5), 1021–1042. https://doi.org/10.1175/JTECH-D-13-00132.1

Fu, J.-X., Wang, W., Shinoda, T., Ren, H.-L., & Jia, X. (2018). Toward understanding the diverse impacts of air-sea interactions on MJO simulations. *Journal of Geophysical Research: Oceans*, *122*, 8855–8875. https://doi.org/10.1002/2017JC013187

Gosnell, R., Fairall, C. W., & Webster, P. J. (1995). The sensible heat of rainfall in the tropical ocean. *Journal of Geophysical Reseach*, *100*, 437–442.

Jacob, D. S., & Koblinsky, C. J. (2013). Effects of precipitation on the upper-Ocean response to a hurricane. *Monthly Weather Review*, *135*, 2207–2225.

Jourdain, N. C., Lengaigne, M., Vialard, J., Madec, G., Menkes, C. E., Vincent, E. M., et al. (2013). Observation-based estimates of surface cooling inhibition by heavy rainfall under tropical cyclones. *Journal of Physical Oceanography*, *43*(1), 205–221. https://doi.org/10.1175/JPO-D-12-085.1

Kilpatrick, T. J., & Xie, S.-P. (2015). ASCAT observations of downdrafts from mesoscale convective systems. *Geophysical Research Letters*, *42*, 1951–1958. https://doi.org/10.1002/2015GL063025

Large, W. G., McWilliams, J. C., & Doney, S. C. (1994). Oceanic vertical mixing: A review and a model with nonlocal boundary layer parameterisation. *Reviews of Geophysics*, *32*(4), 363–403. https://doi.org/10.1029/94RG01872

Madden, R. A., & Julian, P. R. (1971). Detection of a 40-50 day oscillation in the zonal wind in the tropical Pacific. *Journal of the Atmospheric Sciences*, *28*(5), 702–708. https://doi.org/10.1175/1520-0469(1971)028%3C0702:DOADOI%3E2.0.CO;2

Madden, R. A., & Julian, P. R. (1972). Description of global-scale circulation cells in the tropics with a 40-50 day period. *Journal of the Atmospheric Sciences*, *29*(6), 1109–1123. https://doi.org/10.1175/1520-0469(1972)029%3C1109:DOGSCC%3E2.0.CO;2

Moum, J. N., de Szoeke, S. P., Smyth, W. D., Edson, J. B., DeWitt, H. L., Moulin, A. J., et al. (2014). Air–sea interactions from westerly wind bursts during the November 2011 MJO in the Indian Ocean. *Bulletin of the American Meteorological Society*, *95*(8), 1185–1199. https://doi.org/10.1175/BAMS-D-12-00225.1

Moum, J. N., Pujiana, K., Lien, R.-C., & Smyth, W. D. (2016). Ocean feedback to pulses of the Madden–Julian oscillation in the equatorial Indian Ocean. *Nature Communications*, *7*, 13203. https://doi.org/10.1038/ncomms13203

Paulson, C. A., & Simpson, J. J. (1977). Irradiance measurements in the Upper Ocean. *Journal of Physical Oceanography*, *7*(6), 952–956. https://doi.org/10.1175/1520-0485(1977)007%3C0952:IMITUO%3E2.0.CO;2

Price, J. F., Weller, R. A., & Pinkel, R. (1986). Diurnal cycling: Observations and models of the upper ocean response to diurnal heating, cooling, and wind mixing. *Journal of Geophysical Research*, *91*(C7), 8411–8427. https://doi.org/10.1029/JC091iC07p08411

Pujiana, K., Moum, J. N., & Smyth, W. D. (2018). The role of turbulence in redistributing upper-ocean heat, freshwater, and momentum in response to the MJO in the equatorial Indian Ocean. *Journal of Physical Oceanography*, *48*(1), 197–220. https://doi.org/10.1175/JPO-D-17-0146.1

Qian, L., Young, G. S., & Frank, W. M. (1998). A convective wake parameterization scheme for use in general circulation models. *Monthly Weather Review*, *126*(2), 456–469. https://doi.org/10.1175/1520-0493(1998)126%3C0456:ACWPSF%3E2.0.CO;2

Riley Dellaripa, E. M., Maloney, E., & van den Heever, S. C. (2018). Wind–flux feedbacks and convective organization during the November 2011 MJO event in a high-resolution model. *Journal of the Atmospheric Sciences*, *75*(1), 57–84. https://doi.org/10.1175/JAS-D-16-0346.1

Riley Dellaripa, E. M., & Maloney, E. D. (2015). Analysis of MJO wind-flux feedbacks in the Indian Ocean using RAMA buoy observations. *Journal of the Meteorological Society of Japan*, *93A*(0), 1–20. https://doi.org/10.2151/jmsj.2015-021

Rowe, A. K., & Houze, R. A. (2015). Cloud organization and growth during the transition from suppressed to active MJO conditions. *Journal of Geophysical Research: Atmospheres*, *120*, 10,324–10,350. https://doi.org/10.1002/2014JD022948

Saxen, T. R., & Rutledge, S. A. (1998). Surface fluxes and boundary layer recovery in TOGA COARE: Sensitivity to convective organization. *Journal of the Atmospheric Sciences*, *55*(17), 2763–2781. https://doi.org/10.1175/1520-0469(1998)055%3C2763:SFABLR%3E2.0.CO;2

Schlemmer, M., & Hohenegger, C. (2014). The formation of wider and and deeper clouds as a result of cold-pool dynamics. *Journal of the Atmospheric Sciences*, *55*, 2763–2781.

Seigel, R. B., & van den Heever, S. C. (2011). Simulated density current beneath embedded stratified layers. *Journal of the Atmopheric Sciences*, *69*, 2192–2200.
Shinoda, T. (2005). Impact of the diurnal cycle of solar radiation on intraseasonal SST variability in the western equatorial Pacific. *Journal of Climate*, *18*(14), 2628–2636. https://doi.org/10.1175/JCLI3432.1
Shinoda, T., & Hendon, H. H. (1998). Mixed layer modeling of intraseasonal variability in the tropical western Pacific and Indian Oceans. *Journal of Climate*, *11*(10), 2668–2685. https://doi.org/10.1175/1520-0442(1998)011%3C2668:MLMOIV%3E2.0.CO;2
Skyllingstad, E. D., & de Szoeke, S. P. (2015). Cloud-resolving large-eddy simulation of tropical convective development and surface fluxes. *Monthly Weather Review*, *143*(7), 2441–2458. https://doi.org/10.1175/MWR-D-14-00247.1
Sobel, A., Wang, S., & Kim, D. (2014). Moist static energy budget of MJO during DYNAMO. *Journal of the Atmospheric Sciences*, *71*(11), 4276–4291. https://doi.org/10.1175/JAS-D-14-0052.1
Soloviev, A., Lukas, R., & Hacker, P. (2001). An approach to parameterization of the oceanic turbulent boundary layer in the western Pacific warm pool. *Journal of Geophysical Research*, *106*(C3), 4421–4435. https://doi.org/10.1029/2000JC900154
Terai, C., & Wood, R. (2013). Aircraft observations of cold pools under marine stratocumulus. *Atmospheric Chemisty and Physics*, *13*(19), 9899–9914. https://doi.org/10.5194/acp-13-9899-2013
Tompkins, A. M. (2001). Organization of tropical convection in low verticalwind shears: The role of cold pools. *Journal of the Atmospheric Sciences*, *58*(13), 1650–1672. https://doi.org/10.1175/1520-0469(2001)058%3C1650:OOTCIL%3E2.0.CO;2
Torri, G., & Kuang, Z. (2016). A lagrangian study of precipitation-driven downdrafts. *Journal of the Atmospheric Sciences*, *73*(2), 839–854. https://doi.org/10.1175/JAS-D-15-0222.1
Torri, G., Kuang, Z., & Tian, Y. (2015). Mechanisms for convection triggering by cold pools. *Geophysical Research Letters*, *42*, 1943–1950. https://doi.org/10.1002/2015GL063227
Umlauf, L., & Burchard, H. (2003). A generic length-scale equation for geophysical turbulence models. *Jounral of Marine Research*, *61*(2), 235–265. https://doi.org/10.1357/002224003322005087
Umlauf, L., Burchard, H., & Bolding, K. (2005). GOTM—Scientific documentation. Version 3.2 (Tech. Rep. 63). Warnemünde, Germany: Leibniz-Institute for Baltic Sea Research.
Yokoi, S., Katsumata, M., & Yoneyama, K. (2014). Variability in surface meteorology and air-sea fluxes due to cumulus convective systems observed during CINDY/DYNAMO. *Journal of Geophysical Research: Atmospheres*, *119*, 2064–2078. https://doi.org/10.1002/2013JD020621
Yoneyama, K., Zhang, C., & Long, C. N. (2013). Tracking pulses of the Madden–Julian Oscillation. *Bulletin of the American Meteorological Society*, *94*(12), 1871–1891. https://doi.org/10.1175/BAMS-D-12-00157.1
Young, G. S., Perugini, S. M., & Fairall, C. W. (1995). Convective wakes in the equatorial western Pacific during TOGA. *Monthly Weather Review*, *110*, 110–123.
Zhang, C. (2005). Madden-Julian oscillation. *Reviews of Geophysics*, *43*, RG2003. https://doi.org/10.1029/2004RG000158
Zipser, E. J. (1977). Mesoscale and convective-scale downdrafts as distinct components of squall line structure. *Monthly Weather Review*, *105*(12), 1568–1589. https://doi.org/10.1175/1520-0493(1977)105%3C1568:MACDAD%3E2.0.CO;2
Zuidema, P., Li, Z., Hill, R. J., Bariteau, L., Rilling, B., Fairall, C., et al. (2012). On trade wind cumulus cold pools. *Journal of the Atmospheric Sciences*, *69*(1), 258–280. https://doi.org/10.1175/JAS-D-11-0143.1
Zuidema, P., Torri, G., Muller, C., & Chandra, A. (2017). A survey of precipitation-induced atmospheric cold pools over oceans and their interactions with the larger-scale environment. *Surveys in Geophysics*, *38*(6), 1283–1305. https://doi.org/10.1007/s10712-017-9447-x